

# The Magnetic Nature of Coronal Holes

Yi-Ming Wang,\* Scott H. Hawley, Neil R. Sheeley Jr.

Solar wind streams originate from low-density, magnetically open regions of the sun's corona, known as coronal holes. The locations, areal sizes, rotation, and solar-cycle evolution of these regions can be reproduced and understood by applying simple extrapolation models to measurements of the photospheric magnetic field. The surprisingly rigid rotation displayed by many coronal holes suggests that field-line reconnection occurs continually in the corona, despite the high electrical conductivity of the coronal plasma. The magnetic field strengths and field-line divergence rates in coronal holes can be related empirically to the bulk speed and the mass and energy flux densities of the solar wind plasma. Such relations may help to illuminate the physical processes responsible for heating the corona and driving the solar wind.

Coronal holes appear as dark areas in x-ray and extreme-ultraviolet images of the sun, and as light, blurry patches when observed in the He I 10830 Å absorption line. Their importance as sources of high-speed solar wind streams, and of associated geomagnetic activity with a characteristic 27-day recurrence rate, was first recognized in the early 1970s (1). Coronal holes were found to lie within large-scale unipolar areas of the sun, where a single magnetic polarity dominates. Moreover, on the basis of current-free models derived from photospheric magnetograms (2, 3), it was inferred that the magnetic field lines in coronal holes are open, extending outward into the interplanetary medium rather than returning immediately to the sun in the form of closed loops. At the same time, analyses of extreme-ultraviolet images obtained from space showed that the gas densities and temperatures in coronal holes were roughly half the values of those in the adjacent, magnetically closed regions of the corona (4). One of the most intriguing discoveries made during the 1973–1974 Skylab missions was that, in contrast to the underlying photospheric plasma, which rotates differentially, some coronal holes rotate almost rigidly (that is, their rotation rates vary only weakly with latitude). The best known example of this behavior was provided by Coronal Hole 1, a long, boot-shaped structure that was tracked for several months in 1973 (5).

Soon after the Skylab period, it became apparent that coronal holes and their wind streams undergo systematic changes over the 11-year sunspot cycle (6). Through much of the cycle, and in particular near sunspot minimum, the sun's po-

lar regions are dominated by large holes that extend down to a latitude of 60° in each hemisphere. As the Ulysses spacecraft showed when it flew over the solar south pole in 1994, the polar holes are the source of large, persistent wind streams with an average bulk speed of 750 km s<sup>-1</sup> (7). Near the polar hole boundaries, where the oppositely directed magnetic field lines from the two hemispheres come together to form the heliospheric current sheet, the wind speed drops precipitously to only 300 to 400 km s<sup>-1</sup> (8). The eruption of active-region magnetic fields dis-

torts the polar hole boundaries and the shape of the heliospheric current sheet. The resulting equatorward extensions of the polar holes, rotating with the solar equatorial period of ~27 days, produce the recurrent high-speed streams and geomagnetic activity observed during the declining phase of the solar cycle.

At sunspot maximum, the polar holes disappear and are replaced by many small open structures scattered over a wide range of latitudes. These holes, which generally show pronounced differential rotation, are often located near active regions and are characterized by strong magnetic fields and rapidly diverging flux tubes; they may be quite transient in nature. Low wind speeds are prevalent at all latitudes at this time. However, it has been suggested that immediately after sunspot maximum, as magnetic flux surges poleward from the sunspot belts and the polar fields undergo their polarity reversal, very fast wind streams may be generated episodically in the direction of the polar axis (9). The nature of the high-latitude wind near sunspot maximum should become clear

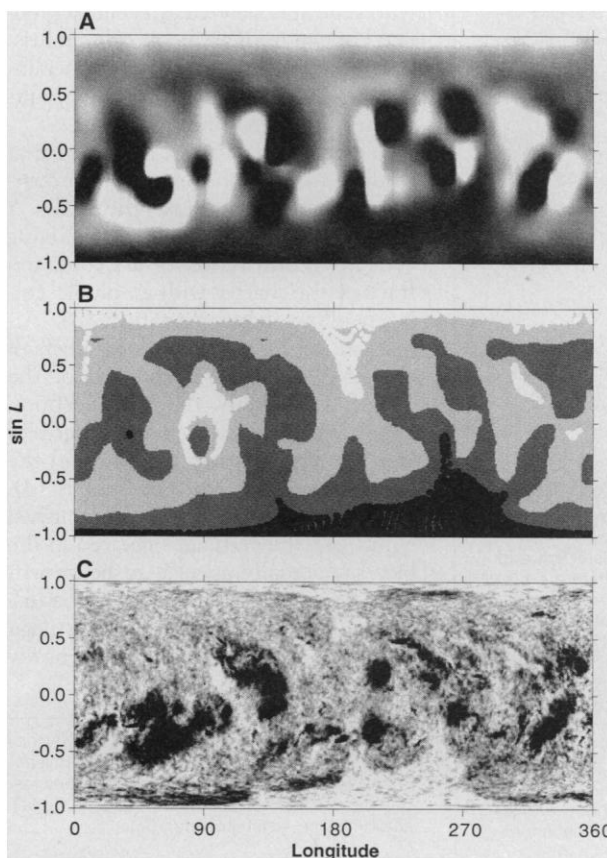


**Fig. 1.** Carrington-format maps for November 1992. (A) Photospheric flux distribution measured by WSO (white, strong positive  $B$ ; black, strong negative  $B$ ). (B) Open and closed magnetic regions derived from (A) with the current-free coronal model (white, positive-polarity open field; black, negative-polarity open field; light gray, positive-polarity closed field; dark gray, negative-polarity closed field). (C) He I 10830 Å intensities recorded at NSO/Kitt Peak (lightest areas, coronal holes; darkest areas, active regions).

Y.-M. Wang and N. R. Sheeley Jr. are at the E. O. Hulburt Center for Space Research, Code 7672, Naval Research Laboratory, Washington, DC 20375-5352, USA. S. H. Hawley is in the Department of Physics, University of Texas, Austin, TX 78712-1081, USA.

\*To whom correspondence should be addressed.

when Ulysses makes its second pass over the poles during 2000–2001.

In this article, we discuss the relation between coronal holes and the sun's large-scale magnetic field. We begin by comparing the magnetically open regions inferred from photospheric field data with the observed locations and evolutionary behavior of coronal holes during the last two sunspot cycles. Next, we show that the rotational properties of coronal holes are consistent with a nearly current-free coronal field that undergoes continual field-line reconnection. We then describe a number of empirical relations between the magnetic fields in coronal holes and the plasma properties of the solar wind, and we consider the implications of these correlations for the heating of the corona and the generation of the solar wind.

### Coronal Holes as Magnetically Open Regions

Although the photospheric field is routinely measured from the ground by means of Zeeman-splitting techniques, the magnetic field in the tenuous solar corona is difficult to observe directly and is usually inferred by applying an extrapolation model to the photospheric data. Here, we use the potential-field source-surface method (10, 11). Let  $r$  denote radial distance from the sun's center,  $L$  denote heliographic latitude, and  $\phi$  denote Carrington longitude (measured westward in the direction of the sun's rotation); the

corresponding three components of the magnetic field vector are  $B_r$ ,  $B_L$ , and  $B_\phi$ . In the potential-field source-surface model, electrical currents are assumed to be negligible in the region between the solar surface ( $r = R_\odot$ ) and a spherical source surface ( $r = R_{ss} = 2.5R_\odot$ ), where the magnetic field is constrained to be purely radial (thereby simulating the effect of the outflowing solar wind plasma as it overcomes the restraining magnetic tension). The further requirement that  $B_r(R_\odot, L, \phi)$  match the observed photospheric flux distribution allows the three components of the potential field to be determined uniquely. By definition, magnetic field lines that extend all the way from the photosphere to the source surface are open, and they continue outward into the heliosphere.

This extrapolation procedure was applied to monthly synoptic photospheric field maps recorded at the Wilcox Solar Observatory (WSO). As an illustrative example, the observed photospheric flux distribution for Carrington rotation 1862 (31 October to 27 November 1992) is shown with a corresponding plot of open field regions derived from these data (Fig. 1, A and B). Comparing the latter plot with a He I 10830 Å map recorded at the National Solar Observatory (NSO/Kitt Peak) during the same 27-day period (Fig. 1C), we see a generally good correspondence between the calculated footpoint locations of open field lines and the observed coronal holes. In the southern hemi-

sphere, both maps show a large structure that represents an equatorward extension of the south polar hole. This negative-polarity lobe was the source of a recurrent high-speed stream observed by Ulysses as it journeyed away from the ecliptic to a heliographic latitude of 35°S between July 1992 and July 1993 (7, 12). The same long-lived stream, recorded in the ecliptic plane by the IMP-8 spacecraft, gave rise to geomagnetic activity with a 27-day period. The positive-polarity open structure or hole straddling the equator near Carrington longitude 90° also produced recurrent geomagnetic activity through the second half of 1992.

We determined the long-term evolution of open field regions at a series of latitudes by applying the coronal extrapolation model to a long sequence of WSO photospheric field maps recorded from August 1976 to April 1995 (Carrington rotations 1645 to 1894) (Fig. 2A). In constructing these multilatitude stack plots, a thin horizontal strip centered at the given latitude was cut out from each footpoint map (like that shown in Fig. 1B), and the strips were stacked on top of each other to form a time-ordered vertical sequence. Corresponding stack plots of observed He I 10830 Å holes are shown in Fig. 2B. The derived patterns of open field regions resemble the observed holes throughout the 1976–1995 interval, although some relatively subtle discrepancies may be seen. In particular, the helium coronal holes tend to be more fragmentary and smaller than

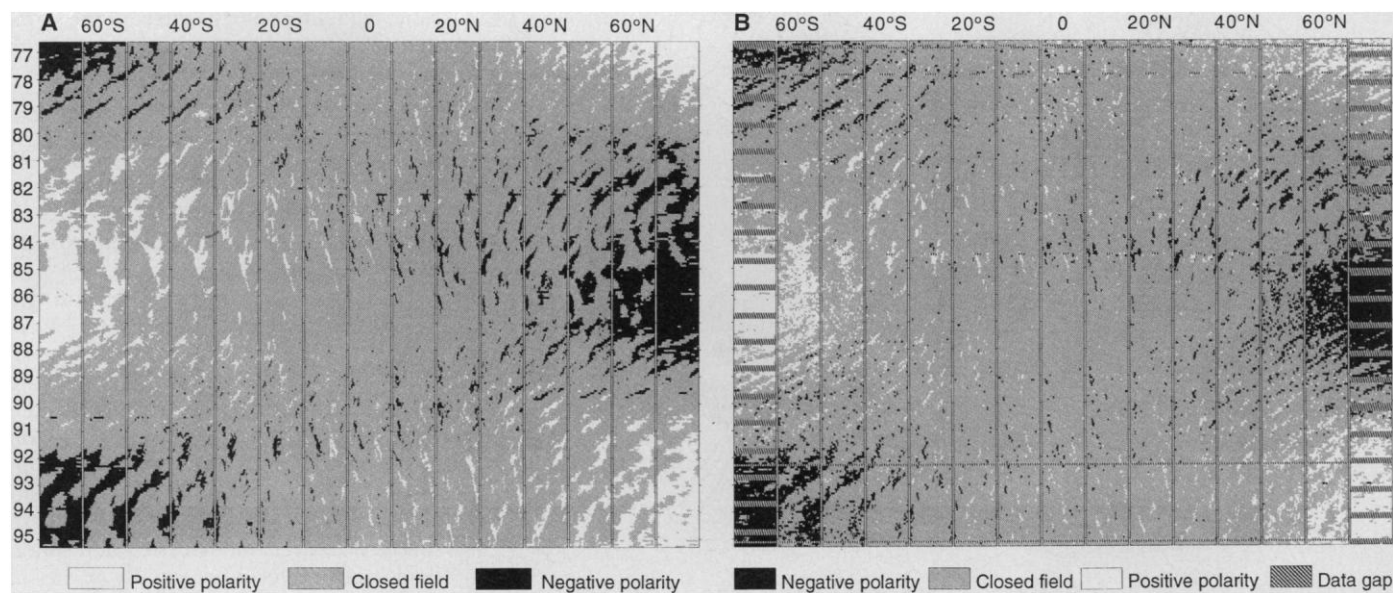


**Fig. 2.** Multilatitude stack plots. **(A)** Long-term evolution of the open field regions derived from the WSO magnetograph measurements; **(B)** long-term evolution of the NSO He I 10830 Å coronal holes. In each latitude panel, Carrington longitude runs from left to right; successive rows of pixels represent successive 27.3-day Carrington rotations. The coronal hole areas in **(B)** were located by applying intensity threshold criteria and smoothing

techniques to the NSO helium synoptic maps, and their polarities were determined from the WSO photospheric field data (which contain less high-latitude noise than do the NSO magnetograph measurements). Stack plots for latitudes poleward of 70° are not shown because observations in those regions are strongly affected by annual variations caused by the sun's 7° axial tilt.

the computed open field regions, presumably because the spatial resolution and instrumental noise of the NSO He I 10830 Å observations are much greater than those of the WSO magnetograph measurements. In contrast, a number of Skylab era studies found that the observed holes were consistently larger than the calculated open field regions, especially at high latitudes (3). This discrepancy can be attributed to the use of noisy polar field measurements and the application of an inappropriate photospheric boundary condition in the earlier potential field extrapolations (11). Hereafter, we will assume that coronal holes are identical to open field regions and use the two terms interchangeably.

The stack plots of Fig. 2 are dominated by large polar holes near sunspot minimum (1976, 1986), which recede and disappear at sunspot maximum (1979–1980, 1989–1990). A prominent gap appears between 1986 and 1988 near the equator, where no coronal holes are present because of the lack of low-latitude sunspot activity. Particularly striking are the ubiquitous slanted patterns of coronal holes. These long-lived

open structures, some of which persist for well over a year, are associated with the eruption and decay of active-region complexes. The magnetic flux of these complexes is gradually dispersed by supergranular convective motions and meridional surface flow to form large-scale unipolar regions (13, 14). The associated coronal holes generate recurrent high-speed streams and are evidently the source of the long-term enhancements in average wind speed, with durations of a few months to more than a year, seen in spacecraft data (15).

Because successive rows of pixels in each stack plot represent successive 27.3-day intervals, the slopes of the patterns are a measure of the rotation rates of the coronal holes in a 27.3-day frame. During the earlier phases of the sunspot cycle, the patterns (when tracked downward in the direction of increasing time) tend to slant strongly to the left, which indicates that the constituent holes are rotating with periods of 28 days or longer, as is characteristic of the high-latitude photosphere. As sunspot activity declines, however, the patterns become nearly vertical or slant to the right, indicating rotation at close to

the sun's 27-day equatorial rate at all latitudes. Thus, the rigid rotation displayed by Coronal Hole 1 during 1973 appears to be a general property of open field regions during the late phases of the sunspot cycle.

### Rotation of Coronal Holes

The following idealized model illustrates the basic mechanism of coronal hole rotation. Assume the presence of a large-scale background photospheric field of the form

$$B_{\text{dipole}}(R_{\odot}, L) = D \sin L \quad (1)$$

with  $D = 1$  G, which represents an axisymmetric dipole flux distribution with a peak field strength of 1 G at the solar poles. In addition, suppose that there is a bipolar magnetic region (BMR) that extends in latitude from  $10^{\circ}\text{N}$  to  $40^{\circ}\text{S}$  and has a longitudinal width of  $120^{\circ}$ :

$$B_{\text{BMR}}(R_{\odot}, L, \phi) =$$

$$\begin{cases} -5 \text{ G}, & -40^{\circ} < L < 10^{\circ}, 120^{\circ} < \phi < 180^{\circ} \\ +5 \text{ G}, & -40^{\circ} < L < 10^{\circ}, 180^{\circ} < \phi < 240^{\circ} \end{cases} \quad (2)$$

This bipolar structure can be regarded as an idealization of a large, decaying active region (or active-region complex) whose flux has been dispersed over a wide area by supergranular convective motions. The initial photospheric field is then given by the superposition

$$B_{\text{ph}}(R_{\odot}, L, \phi) = B_{\text{dipole}}(R_{\odot}, L) + B_{\text{BMR}}(R_{\odot}, L, \phi) \quad (3)$$

We now evolve the photospheric field in time, including only the effect of the surface differential rotation, as described by the classical Newton-Nunn formula

$$\omega(L) = 13.39 - 2.77 \sin^2 L \text{ degrees day}^{-1} \quad (4)$$

As above, we use the current-free approximation to determine the coronal field corresponding to the photospheric flux distribution at any given time.

The simulated coronal holes and their field lines over five 27.3-day rotations are shown in Fig. 3. The BMR distorts the large axisymmetric polar holes associated with the background dipole field: an equatorward extension connects each polar hole with the like-polarity sector of the BMR. The northern hemisphere extension maintains its basic shape throughout the simulation, even though the photospheric field itself rotates differentially at the rate given by Eq. 4. In contrast, the extension of the south polar hole becomes increasingly sheared with time, although even in this case the shearing rate is less than for the underlying photosphere.

To understand the behavior of the polar

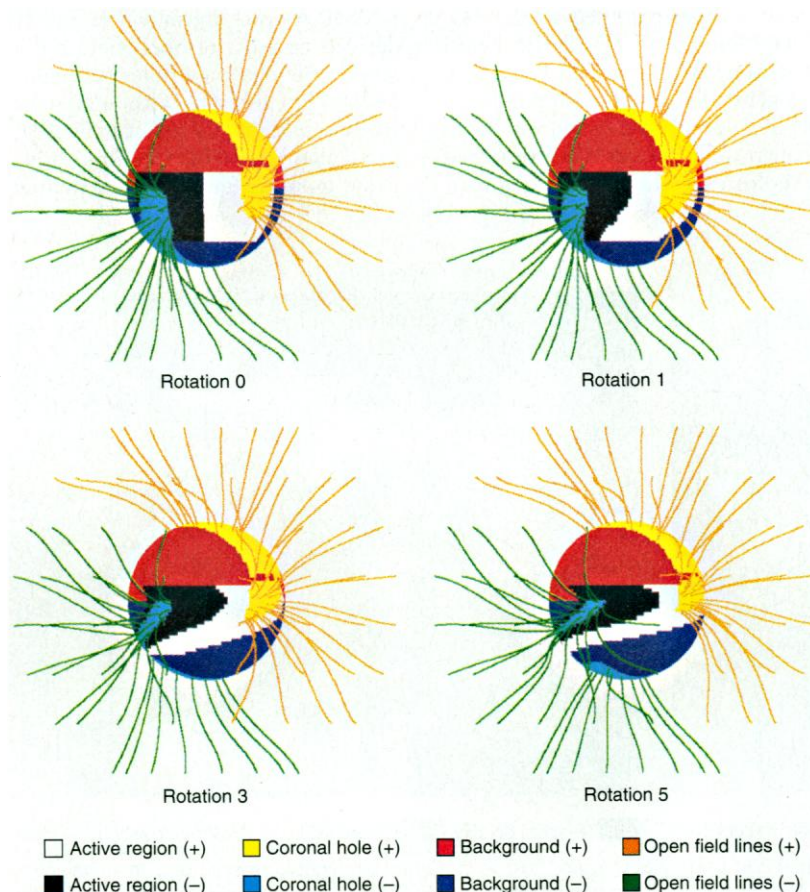


**Fig. 3.** Simulation of rotating polar hole extensions, where the initial photospheric field is the superposition of an axisymmetric dipole and an east-west-oriented BMR confined to the latitude range  $10^{\circ}\text{N}$  to  $40^{\circ}\text{S}$ . The open field lines, their footpoint areas, and the differentially rotating BMR are shown at the initial instant and after one, three, and five 27.3-day rotations.

hole extensions, it is instructive to consider separately the axisymmetric ( $\phi$ -independent) and nonaxisymmetric ( $\phi$ -dependent) components of the initial configuration. If only the background dipole field were present, the open magnetic flux would be confined to axisymmetric polar holes extending down to latitude  $40^\circ$  in each hemisphere (Fig. 4A). On the other hand, if only the BMR were present, the open flux would be confined to the east and west ends of the BMR (Fig. 4B). However, when the background and BMR fields are superposed (Fig. 4C), the resulting hole areas are not the same as those associated with the separate component fields; open field regions are not additive. A neck of open field lines now bridges the  $30^\circ$  wide gap between the north polar hole and the like-polarity sector of the BMR, whereas the polar hole boundary in each hemisphere recedes away from the opposite-polarity sector of the BMR. It may seem paradoxical that these large nonaxisymmetric distortions of the polar hole boundaries occur at latitudes where the photospheric field has a purely axisymmetric ( $\sin L$ ) distribution. However, the locations of the open field regions depend not only on the local photospheric field, but also on the overlying coronal field. The latter in turn depends on the global photospheric flux distribution and is thus generally nonaxisymmetric.

It is now evident why the polar hole extensions do not rotate at the local photospheric rate. Because the background dipole field is purely axisymmetric, the rotation of the coronal field is entirely controlled by the BMR. In particular, any nonaxisymmetric distortion in the current-free coronal field must approximately corotate with the BMR flux that gives rise to the distortion; the same holds for the accompanying distortion in the footpoint (coronal hole) areas. In the idealized limit where all of the BMR flux is concentrated at a single latitude  $L_0$ , the coronal field and the perturbed polar hole boundaries would simply rotate at the rigid rate corresponding to the latitude  $L_0$ . In that case, both the photospheric flux distribution and its current-free

coronal extension would remain exactly stationary in a frame that corotates with the BMR.

The differing evolution of the north and south polar hole extensions in Fig. 3 is a consequence of the latitudinal asymmetry in the BMR. The photospheric flux that produces the distortion in the north polar hole boundary originates mainly from a narrow latitudinal band around the equator (the contribution from the BMR flux located deep in the southern hemisphere is negligible by comparison). Consequently, the northern hemisphere extension rotates quasi-rigidly at approximately the 27-day rate of its low-latitude source region. By contrast, the source of the nonaxisymmetric coronal field in the southern hemisphere is spread between the equator and  $40^\circ\text{S}$ . Because the corresponding photospheric rotation periods range from 26.9 days to as long as 29.4 days, the south polar hole extension shears far more rapidly than does its northern hemisphere counterpart. Nevertheless, the high-latitude boundaries of the south polar hole still rotate faster and more rigidly than does the underlying photosphere, because all of the BMR flux lies equatorward of  $40^\circ\text{S}$ .

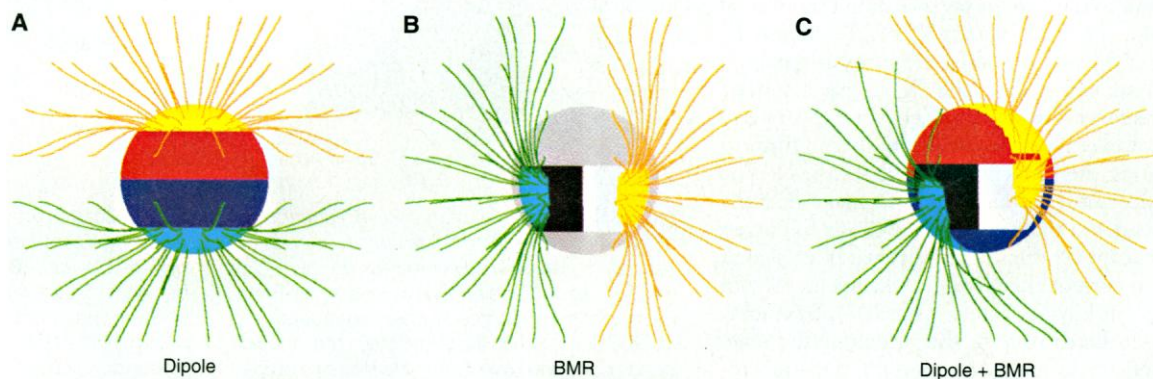
The behavior of the north polar hole extension in Fig. 3 is similar to that observed in Coronal Hole 1, which formed after the eruption of an active-region complex centered at  $\sim 15^\circ\text{S}$  (5, 16). The photospheric flux located at the western edge of this complex had positive polarity, as did the north polar field during 1973. The south polar hole extension in Fig. 3 likewise had its observed Skylab era counterpart in Coronal Hole 5, which became increasingly sheared as positive-polarity flux spread southeastward from the same active-region complex, cutting steadily into the large spur of the negative-polarity south polar hole.

Returning to the slanted coronal hole patterns of Fig. 2, we can now understand why their slopes show systematic changes over the sunspot cycle. As described by the butterfly diagram of sunspot latitudes versus time, activity tends to migrate equatorward as the cycle progresses. During the rising phase of the cycle, active

regions erupt at middle latitudes, where they inject nonaxisymmetric magnetic flux characterized by long rotation periods and thus give rise to sheared polar hole extensions. Slowly rotating coronal holes are also seen just after sunspot maximum, when meridional surface flows carry magnetic flux poleward from the sunspot belts in great surges (17). As activity declines, most of the nonaxisymmetric photospheric flux is confined to low latitudes, where it produces rigidly rotating polar hole extensions and the quasi-vertical patterns seen in the stack plots.

In summary, coronal holes are patterns of open magnetic fields that drift relative to the photospheric plasma. The individual elements of photospheric flux that happen to lie within a hole continue to rotate at the local plasma rate, not at the rate of the pattern. As these magnetic elements are convected across the boundaries of the hole, their flux must be converted from closed to open (when entering the hole) or open to closed (when leaving the hole). In the current-free coronal model, this conversion takes place automatically; indeed, the entire coronal field configuration rearranges itself instantaneously in response to the differential motion of the photosphere, so as to maintain the curl-free condition  $\nabla \times \mathbf{B} = 0$ . The rearrangements involve field-line reconnections in the sense that, if a given pair of photospheric flux elements are connected at time  $t$  by a coronal field line, they will generally not be so connected at a later time  $t'$ ; similarly, opposite-polarity flux elements that are initially unconnected (or open) may become connected to each other as shearing proceeds in accordance with Eq. 4. Such reconnections must take place continually in the actual solar corona, despite the high electrical conductivity that characterizes the coronal plasma. Evidently, the usual assumption that the magnetic flux remains everywhere frozen into the plasma must break down at some locations and on some spatial scale. Although the precise manner in which this breakdown occurs is not well understood, the time scale for reconnection is probably determined by the local Alfvén

**Fig. 4.** Open field regions associated with (A) an axisymmetric dipole flux distribution, (B) a BMR of the form given by Eq. 2, and (C) the superposition of the dipole and the BMR (the initial configuration of Fig. 3). Gray represents zero field; other colors are as in Fig. 3.



speed (the speed at which disturbances propagate along field lines in the presence of a plasma), which is on the order of 1000 km s<sup>-1</sup> in the tenuous solar corona.

### Coronal Magnetic Fields and the Solar Wind

Magnetic fields are generally assumed to play an essential role in heating the corona and accelerating the solar wind, although the physical mechanisms remain unclear (18–20). It is therefore of interest to look for empirical relations between the magnetic fields in coronal holes and observed properties of the solar wind plasma. Consider the flow along a magnetic flux tube that extends from the sun to Earth. Because mass and magnetic flux are conserved along such a tube, the proton flux density at the sun is related to that at Earth by

$$n_0 v_0 = \left( \frac{B_0}{B_E} \right) n_E v_E \quad (5)$$

where  $n$  is the number density of protons (with mass  $m_p$  and mass density  $\rho = nm_p$ ),  $v$  is the bulk wind velocity,  $B$  is the component of the magnetic field in the direction of the flow, and the subscripts 0 and E denote quantities evaluated at the coronal base and at Earth, respectively. The coronal base is defined as the height at which the electron temperature equals  $5 \times 10^5$  K, which corresponds roughly to the top of the chromospheric-coronal transition region. Because radiative energy losses are negligible above the coronal base, the conservation of energy along the sun-Earth flux tube may be written as

$$F_{w0} = \left( \frac{B_0}{B_E} \right) \frac{1}{2} \rho_E v_E^3 \quad (6)$$

where  $F_w$  denotes the total energy flux density of the solar wind, which at Earth is mainly in the form of the bulk kinetic energy  $\rho_E v_E^3/2$  (20).

If  $B_0$ ,  $B_E$ ,  $n_E$ , and  $v_E$  are known, we can use these equations to derive the mass and energy flux densities at the sun. We obtained spacecraft measurements of  $n_E$  and  $v_E$  from the National Space Science Data Center (NSSDC) and converted the hourly data to daily averages spanning the interval May 1976 to January 1994. To obtain  $B_0$  and  $B_E$ , we again used the current-free model to extrapolate the WSO photospheric field to  $r = R_{ss} = 2.5R_\odot$ ; beyond this radius, however, we introduced sheet currents along the surfaces where  $B_r = 0$  (21). The effect of these currents is to make  $B_r$  independent of latitude and longitude for large  $r$  (except for the sudden reversal of its sign at the current sheet itself), in agreement with recent Ulysses observations (22). By tracing from Earth back to the sun along the magnetic field and correcting for the sun's ro-

tation during the propagation time  $\Delta t = (215R_\odot)/v_E$ , we determined a net areal expansion factor  $B_0/B_E$  corresponding to each daily value of  $n_E$  and  $v_E$ , and we thus obtained  $n_0 v_0$  and  $F_{w0}$  at the sun from Eqs. 5 and 6.

Both the mass and energy flux densities at the sun tend to increase approximately linearly with increasing magnetic field strength (Fig. 5). In contrast, there appears to be almost no systematic relation between  $B_0$  and the solar wind speed at Earth,

$$v_E \approx \left( \frac{2F_{wE}}{\rho_E v_E} \right)^{1/2} = \left( \frac{2F_{w0}}{\rho_0 v_0} \right)^{1/2} \quad (7)$$

In addition to  $B_0$ , another useful parameter for characterizing the magnetic field near the sun is the flux tube expansion factor (23, 24), which we define as

$$f_{ss} = \left( \frac{R_\odot}{R_{ss}} \right)^2 \left( \frac{B_0}{B_{ss}} \right) \quad (8)$$

where  $B_{ss}$  is the field strength at the point where the sun-Earth flux tube intersects the source surface  $r = R_{ss} = 2.5R_\odot$ ;  $f_{ss}$  thus represents the factor by which the flux tube expands between the coronal base and the source surface. Both the mass and energy flux densities at the coronal base tend to increase with increasing expansion factor near the

sun (Fig. 6). However, because  $\rho_0 v_0$  rises more steeply with  $f_{ss}$  than does  $F_{w0}$ , the energy per proton—and thus the wind speed at Earth,  $v_E \approx (2F_{w0}/\rho_0 v_0)^{1/2}$ —tends to decline as the expansion factor increases (24).

What is the physical significance of these empirical relations between the coronal magnetic field and the plasma properties of the solar wind? Energy balance considerations imply that the energy flux density  $F_{m0}$  required to heat the coronal hole plasma must approximately offset the gravitational energy flux near the coronal base, given by  $-\rho_0 v_0 GM_\odot/R_\odot$  (25). Because  $\rho_0 v_0$  increases roughly linearly with  $B_0$  (Fig. 5A), the coronal heating rate  $F_{m0}$  must vary in proportion to the field strength at the coronal base. Moreover, Fig. 5B shows that the total energy flux density  $F_{w0}$ —which may include, for example, an Alfvén wave contribution that accelerates the wind to high speeds (18–20, 26)—is likewise roughly proportional to  $B_0$ . These empirical results are thus consistent with the widely held theoretical supposition that the heating of the corona and the acceleration of the solar wind are in some way related to the sun's magnetic field.

The tendency for the mass flux density at the sun to increase monotonically with the

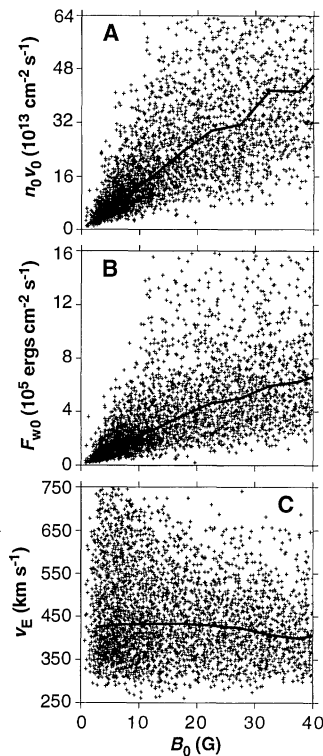


**Fig. 5.** Scatterplots of magnetic field strength  $B_0$  at the sun versus (A) ion flux density  $n_0 v_0$  at the sun, (B) total solar wind energy flux density  $F_{w0}$  at the sun, and (C) solar wind speed  $v_E$  at Earth. Each cross represents a daily average during 1976–1994. Solid lines indicate the median trends calculated over 5-G-wide intervals of  $B_0$ .

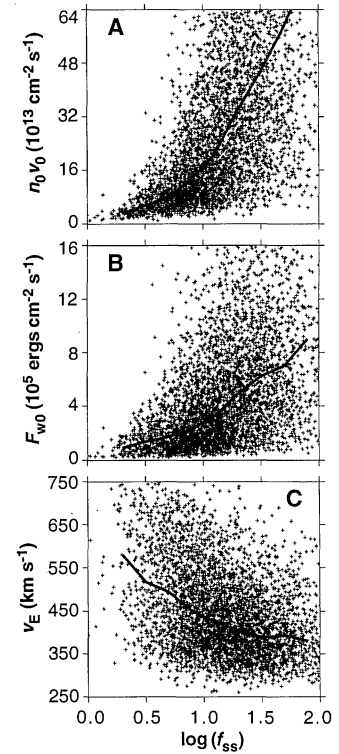


**Fig. 6.** Scatterplots of the logarithmic expansion factor  $\log(f_{ss})$  at the sun versus (A) ion flux density  $n_0 v_0$  at the sun, (B) total solar wind energy flux density  $F_{w0}$  at the sun, and (C) solar wind speed  $v_E$  at Earth. Each cross represents a daily average during 1976–1994. Solid lines indicate the median trends calculated over intervals of 0.2 log units.

expansion factor (Fig. 6A) is predicted by solar wind models in which the coronal temperature is assumed to be fixed (27). If the energy flux density at the sun were also assumed to be invariant, the energy per proton, and thus the wind speed at Earth  $v_E \approx (2F_{w0}/\rho_0 v_0)^{1/2}$ , would tend to decrease with increasing  $f_{ss}$ , as observed (Fig. 6C). However,  $F_{w0}$  in fact increases with  $f_{ss}$  (Fig. 6B), but not as steeply as does  $\rho_0 v_0$  (Fig. 6A). This difference in the average slopes gives rise to the inverse relation between  $v_E$  and  $f_{ss}$ .

A number of effects may contribute to the large scatter about the median trends in Figs. 5 and 6. Small-scale magnetic structure, either spatially unresolved by the WSO magnetograph or not described by the current-free coronal model, may be present near the coronal base. Also, changes in the photospheric field on time scales less than the solar rotation period are not recorded by the monthly synoptic maps. Interactions between wind streams propagating at different speeds have not been taken into account, nor have coronal mass ejections (which occur frequently near sunspot maximum) been removed from the plasma data. Perhaps most important, the wide scatter of the points in Figs. 5 and 6 may indicate that the heating and acceleration of the solar wind are dependent on other, as yet unknown, physical parameters in addition to  $B_0$  and  $f_{ss}$  (28).

### Concluding Remarks

Coronal holes are continually evolving structures that directly connect the sun to the heliosphere, and as such they are the main source of the interplanetary plasma and magnetic field and of their long-term variation. By combining solar magnetograph measurements with simple coronal extrapolation models, it is possible to deduce when and where these magnetically open regions form, how they rotate and evolve, and what relations exist between them and the properties of the solar wind.

Although this article has been concerned mainly with the large-scale magnetic properties of coronal holes, finer-scale structures that are also present in holes may provide further clues about the heating processes that take place within them (18, 29). The best known of these features are the polar plumes, which appear as long, faint rays in eclipse and coronagraph images (30) and as shorter spikes or curtains in the extreme ultraviolet (31). Energy balance models indicate that an extra source of heating must be present at the base of a plume to account for its high gas density relative to the background hole (26). A possible heating mechanism may be field-line reconnection between small magnetic bipoles and nearby unipolar flux concentrations located at the supergranular network

junctions. Continual small-scale network activity has also been suggested as the general heating source of coronal holes (18).

Another interesting question concerns the origin of elemental abundance variations in the solar wind. High-speed streams have a composition more like that of the photosphere than does slow wind, which is relatively enriched in easily ionized elements like magnesium (32). Slow wind is associated with the boundary regions of large coronal holes and with the small open field regions that are prevalent around sunspot maximum (13), whereas magnesium-rich plasma is found primarily in magnetically closed regions of the corona (33). Presumably, this plasma is released into the heliosphere by reconnection between the closed magnetic loops and the adjacent regions of rapidly diverging open field lines, which are the sources of the slow wind. Such exchanges must continually take place at the boundaries of coronal holes as the photospheric footpoint areas are subjected to rotational shearing and random convective motions.

A principal objective in the study of coronal holes is the development of improved techniques for forecasting high-speed solar wind streams and associated geomagnetic activity. Especially promising in this regard is the inverse correlation found between the solar wind speed at Earth and the flux tube expansion factor at the sun. In principle, routine ground-based observations of the photospheric magnetic field can enable predictions of whether the wind speed at Earth is likely to be high or low on a given day. The reliability of the predictions will depend on an understanding of the origin of the scatter present in Fig. 6C; such an understanding should emerge when the physical processes responsible for accelerating the solar wind are more fully clarified.

### REFERENCES AND NOTES

- For summary articles, see J. B. Zirker, Ed., *Coronal Holes and High Speed Wind Streams* (Colorado Associated Univ. Press, Boulder, 1977). For an introductory account, see H. Zirin, *Astrophysics of the Sun* (Cambridge Univ. Press, Cambridge, 1988), pp. 255–259.
- M. D. Altschuler, D. E. Trotter, F. Q. Orrall, *Sol. Phys.* **26**, 354 (1972).
- R. H. Levine, M. D. Altschuler, J. W. Harvey, B. V. Jackson, *Astrophys. J.* **215**, 636 (1977); G. W. Pneuman, S. F. Hansen, R. T. Hansen, *Sol. Phys.* **59**, 313 (1978).
- R. H. Munro and G. L. Withbroe, *Astrophys. J.* **176**, 511 (1972); G. L. Withbroe and Y.-M. Wang, *Sol. Phys.* **27**, 394 (1972).
- A. F. Timothy, A. S. Krieger, G. S. Vaiana, *Sol. Phys.* **42**, 135 (1975).
- J. W. Harvey and N. R. Sheeley Jr., *Space Sci. Rev.* **23**, 139 (1979); A. J. Hundhausen, R. T. Hansen, S. F. Hansen, *J. Geophys. Res.* **86**, 2079 (1981); V. N. Obridko and B. D. Shelting, *Sol. Phys.* **124**, 73 (1989); P. Navarro-Peralta and A. Sanchez-Ibarra, *ibid.* **153**, 169 (1994).
- J. L. Phillips *et al.*, *Science* **268**, 1030 (1995).
- W. A. Coles *et al.*, *Nature* **286**, 239 (1980); X.-P. Zhao and A. J. Hundhausen, *J. Geophys. Res.* **86**, 5423 (1981); G. Newkirk Jr. and L. A. Fisk, *ibid.* **90**, 3391 (1985); R. Bruno, U. Villante, B. Bavassano, R. Schwenn, F. Mariani, *Sol. Phys.* **104**, 431 (1986).
- Y.-M. Wang, N. R. Sheeley Jr., A. G. Nash, *Nature* **347**, 439 (1990).
- K. H. Schatten, J. M. Wilcox, N. F. Ness, *Sol. Phys.* **6**, 442 (1969); J. T. Hoeksema, thesis, Stanford University (1984).
- Y.-M. Wang and N. R. Sheeley Jr., *Astrophys. J.* **392**, 310 (1992).
- J. L. Phillips *et al.*, *Geophys. Res. Lett.* **21**, 1105 (1994).
- Y.-M. Wang and N. R. Sheeley Jr., *Astrophys. J.* **365**, 372 (1990).
- V. Bumba, M. Klvana, J. Sykora, *Astron. Astrophys.* **298**, 923 (1995).
- J. D. Richardson, K. I. Paularena, J. W. Belcher, A. J. Lazarus, *Geophys. Res. Lett.* **21**, 1559 (1994); P. R. Gazis, J. D. Richardson, K. I. Paularena, *ibid.* **22**, 1165 (1995).
- Y.-M. Wang and N. R. Sheeley Jr., *Astrophys. J.* **414**, 916 (1993).
- R. F. Howard and B. J. LaBonte, *Sol. Phys.* **74**, 131 (1981); V. I. Makarov and K. R. Sivaraman, *ibid.* **119**, 35 (1989); Y.-M. Wang, A. G. Nash, N. R. Sheeley Jr., *Astrophys. J.* **347**, 529 (1989).
- E. N. Parker, *Astrophys. J.* **372**, 719 (1991); W. I. Axford and J. F. McKenzie, in *Solar Wind Seven*, E. Marsch and R. Schwenn, Eds. (Pergamon, Oxford, 1992), pp. 1–5.
- J. V. Hollweg, *Rev. Geophys. Space Phys.* **16**, 689 (1978); J. V. Hollweg, *J. Geophys. Res.* **91**, 4111 (1986).
- E. Leer, T. E. Holzer, T. Flå, *Space Sci. Rev.* **33**, 161 (1982).
- K. H. Schatten, *Cosmic Electrodyn.* **2**, 232 (1971); Y.-M. Wang and N. R. Sheeley Jr., *Astrophys. J.* **447**, L143 (1995).
- A. Balogh *et al.*, *Science* **268**, 1007 (1995).
- R. H. Munro and B. V. Jackson, *Astrophys. J.* **213**, 874 (1977); R. A. Kopp and T. E. Holzer, *Sol. Phys.* **49**, 43 (1976); S. T. Suess, A. K. Richter, C. R. Winge, S. F. Nerney, *Astrophys. J.* **217**, 296 (1977).
- R. H. Levine, M. D. Altschuler, J. W. Harvey, *J. Geophys. Res.* **82**, 1061 (1977); Y.-M. Wang and N. R. Sheeley Jr., *Astrophys. J.* **355**, 726 (1990); *ibid.* **372**, L45 (1991).
- Ø. Sandbæk, E. Leer, V. H. Hansteen, *Astrophys. J.* **436**, 390 (1994).
- G. L. Withbroe, *ibid.* **325**, 442 (1988); J. V. Hollweg and W. Johnson, *J. Geophys. Res.* **93**, 9547 (1988); Y.-M. Wang, *Astrophys. J.* **410**, L123 (1993); *ibid.* **435**, L153 (1994); S. R. Habbal, R. Esser, M. Guhathakurta, R. R. Fisher, *Geophys. Res. Lett.* **22**, 1465 (1995).
- T. E. Holzer and E. Leer, *J. Geophys. Res.* **85**, 4665 (1980).
- V. N. Obridko, A. F. Kharshiladze, B. D. Shelting, *Astron. Rep.* **39**, 95 (1995).
- K. L. Harvey, *Aust. J. Phys.* **38**, 875 (1985); S. R. Habbal, *Ann. Geophys.* **10**, 34 (1992); D. Moses *et al.*, *Astrophys. J.* **430**, 913 (1994).
- K. Saito, *Publ. Astron. Soc. Jpn.* **17**, 1 (1965); G. Newkirk Jr. and J. W. Harvey, *Sol. Phys.* **3**, 321 (1968); S. Koutchmy, *ibid.* **51**, 399 (1977); R. R. Fisher and M. Guhathakurta, *Astrophys. J.* **447**, L139 (1995).
- J. D. Bohlin, N. R. Sheeley Jr., R. Tousey, in *Space Research XV*, M. J. Rycroft, Ed. (Akademie, Berlin, 1975), pp. 651–656; I. A. Ahmad and G. L. Withbroe, *Sol. Phys.* **53**, 397 (1977); K. G. Widing and U. Feldman, *Astrophys. J.* **392**, 715 (1992); Y.-M. Wang and N. R. Sheeley Jr., *ibid.* **452**, 457 (1995).
- J. Geiss, G. Gloeckler, R. von Steiger, *Space Sci. Rev.* **72**, 49 (1995); J. Geiss *et al.*, *Science* **268**, 1033 (1995).
- N. R. Sheeley Jr., *Astrophys. J.* **440**, 884 (1995).
- We thank J. W. Harvey (NSO/Kitt Peak) for the He I 10830 Å synoptic maps and J. T. Hoeksema (WSO/Stanford University) for the photospheric field data. We also thank our former summer students, D. F. Acton, D. L. Aronstein, and D. M. Hurley, for their help in developing the computer algorithm to identify helium coronal holes. Supported by the National Aeronautics and Space Administration, the Office of Naval Research, and the Naval Research Laboratory Summer Student Program (S.H.H.).